Full-Spectrum Carbon Dots Electroluminescent White Light-Emitting Diodes with a Record Color Rendering Index of 94

Dan Li, Zhibin Wang,* Song Zheng, Naizhong Jiang, Chengcai Feng, Ximing Wu, Hailiang Huang, Tao Pang, Lingwei Zeng, Ruidan Zhang, Feng Huang, and Daqin Chen*

Carbon dots (CDs) are emerging as promising nanomaterials for next-generation white electroluminescent devices due to their high photoluminescence quantum yield (PLQY), broad emission spectrum, and compatibility with solution-processed methods. However, current CD-based white light-emitting diodes (CDs-WLEDs) heavily rely on costly commercial host materials and struggle with low color rendering index (CRI). Herein, a "dual-phase CDs emitter" strategy is introduced to achieve full-spectrum white light emission, without employing commercial host materials. As a proof of concept, CDs are synthesized with broadband green emission and nearly 100% PLQY. Spectroscopic and structural analyses confirm that their luminescence originates from molecular state emission. By combining these green CDs with carbon quantum dot organic frameworks capable of dual blue and red emissions, white light is successfully produced with a record CRI of 94 and color coordinates of (0.32, 0.34). This approach provides a cost-effective and efficient pathway for developing high-performance WLEDs that rely exclusively on CDs.

D. Li, Z. Wang, S. Zheng, N. Jiang, C. Feng, X. Wu, H. Huang, R. Zhang, F. Huang, D. Chen
College of Physics and Energy
Fujian Provincial Key Laboratory of Quantum Manipulation and New Energy Materials
Fujian Normal University
Fuzhou 350117, China
E-mail: zhibinwang@fjnu.edu.cn; dqchen@fjnu.edu.cn

T. Pang
Huzhou Key Laboratory of Materials for Energy Conversion and Storage
College of Science
Huzhou University
Huzhou, Zhejiang 313000, P. R. China

L. Zeng
School of Chemistry and Chemical Engineering
Hunan University of Science and Technology
Xiangtan, Hunan 411201, P. R. China

D. Chen
Fujian Provincial Collaborative Innovation Center for Advanced High-Field Superconducting Materials and Engineering
Fuzhou 350117, China

D. Chen
Fujian Provincial Engineering Technology Research Center of Solar Energy Conversion and Energy Storage
Fuzhou 350117, China

1. Introduction

The backlight display and solid-state lighting industries have been striving for high-quality WLEDs that meet the demands for high energy conversion efficiency, high CRI, low cost, and long operational lifetime.[1] Currently, commercial WLEDs are primarily produced using blue LED chips coupled with yellow rare-earth based phosphors, a process that relies on expensive epitaxy growth techniques.[2] Over the past few decades, quantum dots have emerged as promising luminescent materials due to their outstanding optoelectronic properties, including high PLQY, tunable emission spectra, and high color purity.[3] Additionally, quantum dots are easily synthesized, cost-effective, and amenable to solution processing, which could lead to lightweight, low-cost, and structurally simple lighting technologies. However, high-performance quantum dot-based WLEDs typically depend on cadmium or lead, both of which are toxic heavy metals, limiting their commercial viability.[4] Furthermore, the full-width at half-maximums (FWHM) of conventional quantum dots is typically within 30 nm, which may not be suitable for producing white light with the required broadband emission spectrum.[5]

Carbon dots, as a class of 0D nanocarbons, typically have a wide emission spectrum and are free of heavy metals, making them an ideal candidate for WLEDs technology with high CRI.[6,7] Although a large number of CDs have been used in WLEDs, most of them are used as phosphors coupled with GaN-based blue or ultraviolet (UV) chips.[8] Therefore, abandoning the traditional LED chips and employing CDs as the emissive material for electroluminescent white light is the most promising way for flat-panel displays and lighting applications.[9] CDs-based electroluminescent device typically adopts a sandwich structure, in which the emitter can be composed of pure CDs or CDs/organic semiconductors host-guest complexes.[10] One of the key challenges facing CDs-LEDs is the difficulty in achieving high CRI white light. This issue arises primarily from the reliance on commercial blue host materials combined with yellow CDs, which results in gaps in the sky blue and red regions of the spectrum. For instance, our group previously used commercial

polyvinyl carbazole and poly[(9,9-dioctylfluorenyl-2,7-diyl)-alt-(4,4′-(N-(4-butylphenyl)))] (TFB) polymers with yellow CDs to create color temperature-adjustable CDs-based WLEDs.[11] To further improve CRI, we explored the use of an exciplex host with deep-red CDs, achieving a CRI of up to 94.[12] However, most current CDs-WLEDs depend on expensive organic polymers or small-molecule materials, which presents a significant barrier to large-scale, cost-effective commercialization.

Using pure CDs as the emitting layer for WLEDs offers a simpler and cost-effective alternative, as it eliminates the need for expensive polymer host materials. In 2010, Wang et al. reported the first WLED based on pure CDs, achieving white light with Commission Internationale de L'Eclairage (CIE) coordinates of (0.40, 0.43) and a CRI of 82.[13] However, due to the insulating long-chain 1-hexadecylamine on the surface of the CDs, charge carrier injection was hindered, limiting the brightness to only 35 cd m^{-2} and resulting in a high turn-on voltage (V_t) of 6 V. Since then, a few other studies have explored pure CDs as an emitter for WLEDs, but the performance and CRI still lag behind devices using host-guest systems. Two main challenges contribute to this gap: first, CDs tend to aggregate, causing fluorescence quenching and low PLQY, which necessitates the development of solid-state luminescent CD materials. Second, the emission spectrum of single-component CDs still falls short of the broad spectrum required for white light. Recent advances in CD structure design have addressed some of these issues. For example, Tan et al. used a triphenylamine structure to inhibit π-π stacking in CDs, enhancing their solid-state luminescence properties and enabling bright orange and green emissions in pure CDs-based LEDs.[14] Additionally, Shi et al. developed carbon quantum dot organic frameworks (CDOFs) that suppress aggregation-induced quenching (AIQ), resulting in high-PLQY films and red CD-LEDs with an external quantum efficiency (EQE) of 5.6%.[15]

In this study, we present a strategy for achieving high-CRI WLEDs using pure CDs as emitters. The emitters are fabricated through a solution-processed method involving two types of CDs. The first type emits both blue and red light and features a unique framework structure that effectively suppresses AIQ in the solid state. To complete the emission spectrum, we synthesized green CDs with a near-unity PLQY, attributed to their molecular-state luminescence. By combining these two types of CDs, we developed a "dual-phase CDs emitter" through a simple solution-processing technique. This emitter exhibits full-spectrum emission covering the red, green, and blue spectral regions. The resulting WLED achieved CIE coordinates of (0.32, 0.34) and a CRI of 94, representing the highest performance reported to date for a pure-CD-based WLED.

2. Results and Discussion

A common approach to creating CDs-based WLEDs involves combining a commercial blue host with CDs that emit broadband yellow or orange light. However, this method requires costly host materials and typically results in low CRI. Here, we present a simple strategy to achieve white emission using pure CDs by combining two types of CDs that emit in the primary color—red, green, and blue—while maintaining strong solid-state emission characteristics. Building on our prior work with CDs-based LEDs, we selected CDOFs with dual emission peaks as the blue

and red components and synthesized bright green CDs as the green component. This strategy is guided by several key considerations: i) these two types of CDs provide full RGB primary colors and a broad emission spectrum, enabling high-CRI white emission; ii) CDOFs exhibit strong solid-state luminescence, effectively serving as a host to mitigate the AIQ effect; and iii) their excellent film-forming and solution-processing properties facilitate the easy preparation of a composite emissive layer from both types of CDs.

Before fabricating the WLEDs, it is essential to first characterize the structural and optical properties of the two types of CDs. The optical and structural properties of CDOFs have been extensively discussed in our previous work, while the green carbon dots (G-CDs) have not been reported.[15] Therefore, the following section focuses on the characterization of G-CDs.

The synthesis of G-CDs, as shown in **Figure 1a**, involves solvothermal reactions between 1,8-naphthalic anhydride (1,8-NA) and o-phenylenediamine (oPD). 1,8-NA and oPD were chosen as carbon (C) and nitrogen (N) dopant precursors due to their molecular structure, which facilitates the formation of the sp^2 skeleton and incorporation of N atoms into the sp^3 structure. The reaction, carried out in a mixture of N,N-dimethylformamide (DMF), and deionized water at 200 °C for 8 h, yielded three types of CDs with distinct colors. After purification by silica column chromatography, the CDs were redispersed in toluene for further characterization. The synthesized CDs emitted blue fluorescence (denoted "B-CDs") when 1,8-NA was used as the precursor, yellow fluorescence ("Y-CDs") when oPD alone was used, and green fluorescence ("G-CDs") when both 1,8-NA and oPD were combined.

Figure 1b shows the UV–vis absorption spectra of the three CD samples, the three samples exhibit distinct absorption bands between 300 to 400 nm. These bands correspond to n-π* transitions associated with molecular state transition involving C═O/C═O or C─N/C═N structures.[16,17] The photoluminescence (PL) emission peaks of the B-, G-, and Y-CDs were recorded at 405, 500, and 555 nm, with FWHM values of 78.1, 124.6, and 84.1 nm, respectively (Figure 1c). Notably, the PL spectra of B-CDs exhibit excitation-dependent behavior (Figure S1, Supporting Information), indicating the presence of numerous surface defects. Time-resolved photoluminescence (TRPL) analysis of B-CDs revealed a double-exponential decay with a short lifetime of 1.48 ns, which is attributed to radiative recombination from intrinsic and surface states (Figure 1d).[7,18] In contrast, the G-CDs and Y-CDs display excitation-independent PL emissions, suggesting a single luminescence center for each. TRPL measurements for G-CDs and Y-CDs showed single-exponential decays with lifetimes of 10.48 and 12.23 ns, respectively. The absolute PLQYs of B-, G-, and Y-CDs were determined to be 8.99, 97.03, and 17.19%, respectively, using an integrating sphere under optimal excitation wavelengths (Figure S2, Supporting Information).

Transmission electron microscopy (TEM) images (Figure 1e–g) reveal that the CDs are uniformly dispersed with particle sizes of ≈2.02 nm for B-CDs, 1.82 nm for G-CDs, and 2.08 nm for Y-CDs. The TEM and high-resolution TEM images of the three selected samples are shown in Figure S3 (Supporting Information). All of the three types of CDs exhibited identical well-resolved lattice fringes with a d spacing of 0.21 nm, corresponding to the (100) in-plane lattice of graphene. Among
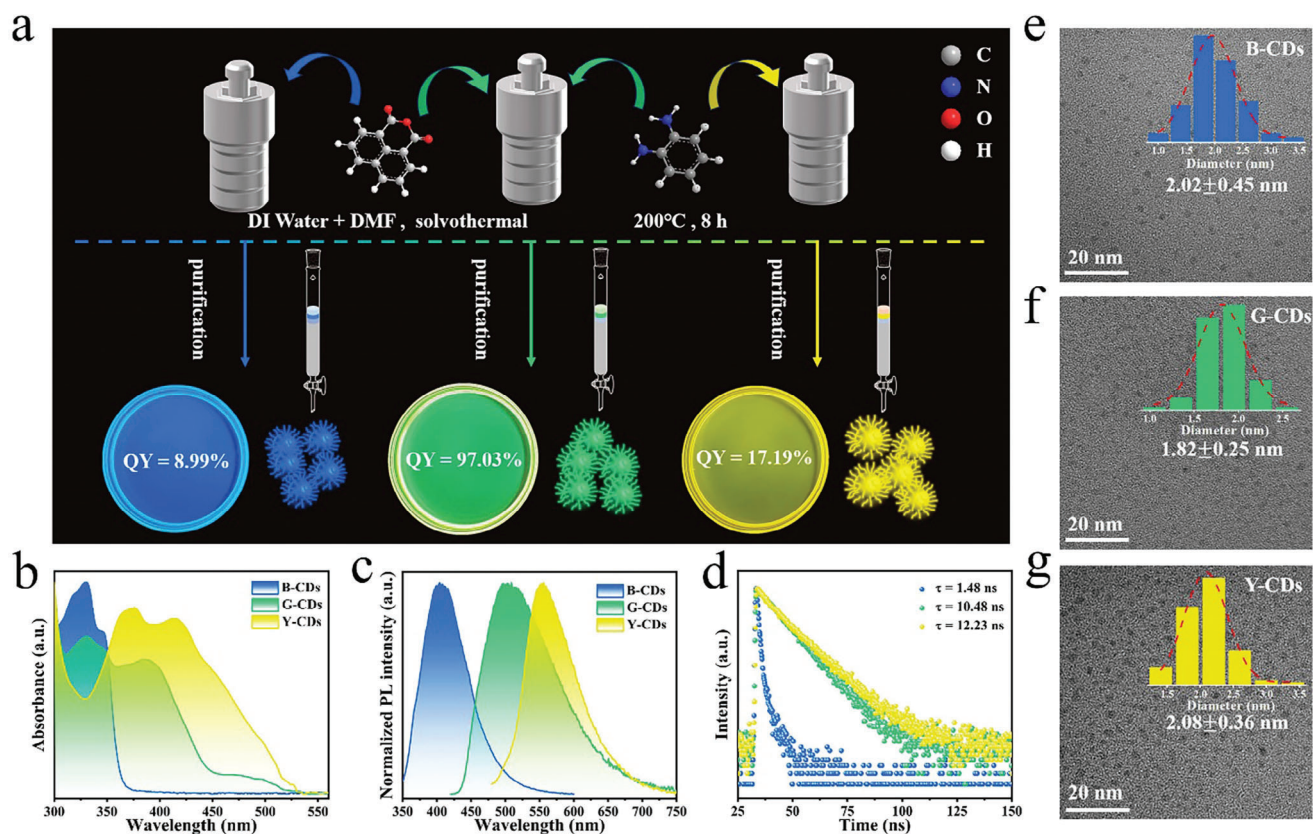
**ADVANCED
SCIENCE NEWS**

www.advancedsciencenews.com

**ADVANCED
FUNCTIONAL
MATERIALS**

www.afm-journal.de

Figure 1. a) Schematic diagram illustrating the preparation of B-CDs, G-CDs, and Y-CDs, along with photographs of their toluene solutions under ultraviolet (UV) light. b) UV–vis absorption spectra, c) photoluminescence (PL) spectra, and d) PL decay curves of B-CDs, G-CDs, and Y-CDs solutions. e–g) Transmission electron microscopy (TEM) images of B-CDs, G-CDs, and Y-CDs. Insets show the corresponding diameter histograms for different CDs.

these, the G-CDs exhibit a less defined structure, likely due to the presence of additional functional groups or attached small molecules on their surface.[8] Raman spectroscopy analysis (Figure S4, Supporting Information) shows characteristic peaks at 1360 cm^{-1} (D-band) and 1600 cm^{-1} (G-band), corresponding to carbon defects/disorder and the in-plane stretching vibrations of sp^2 carbon domains, respectively.[19] The intensity ratios (I_G/I_D) for B-, G-, and Y-CDs are 0.96, 0.70, and 1.04, respectively. This indicates that G-CDs have the lowest degree of graphitization, a finding consistent with the structural observations from TEM analysis.[20]

The near-unity PLQY of the synthesized G-CDs prompted us to conduct extensive characterizations to investigate the chemical structure. The X-ray diffraction pattern depicts two peaks at 23° and 44.6°, corresponding to the (002) and (100) of planes of a graphitic structure (Figure S5a, Supporting Information). The broad peak at 23°, with a d-spacing of 0.32 nm, further confirms the small particle size of the G-CDs.[21] The chemical composition of G-CDs was determined by Fourier transform infrared (FTIR) spectroscopy, as shown in Figure S5b (Supporting Information). Peaks at 3116 and 1237 cm^{-1} indicate sp^3 N—H and C—N stretching and bending vibrations, respectively, while peaks at 1692 and 1547 cm^{-1} correspond to sp^2 C=N and C=C stretching and skeletal vibrations, suggesting a polyaromatic structure with surface N groups.[22]

We found that G-CDs can be synthesized efficiently via a hydrothermal reaction between 1,8-NA and oPD, yielding broadband green emission across a wide range of precursor feed ratios (**Figure 2a**). When the precursor mixture is dominated by 1,8-NA, the resulting CDs exhibit a strong absorption band at ≈330 nm, closely resembling the absorption spectra of B-CDs (Figure 2b). This peak likely arises from the n-π* transition of C=O and C—O groups of the surface state, given the abundance of O-containing functional groups in 1,8-NA.[17] In contrast, when oPD is the predominant precursor, a pronounced absorption band near 380 nm emerges. Despite these variations in absorption spectra, the PL spectra and fluorescence lifetimes of G-CDs synthesized under different feed ratios remain consistent (ranging from 10.41 to 10.59 ns), indicating that their fluorescence originates from the same luminescent center (Figure 2c).

To further investigate, we varied the synthesis temperature and found no significant shift in emission peak positions (Figure S6, Supporting Information). This observation suggests that the emission mechanism is unrelated to conjugation effects and is instead driven by molecular state fluorescence.[23] Notably, recent studies on oPD-derived CDs predominantly report molecular state emissions in long-wavelength regions, such as red and yellow, while green emission with high PLQY (>80%) remains rare.[8,24,25] We hypothesize that a fluorescent molecule, 7H-Benzimidazo[2,1-a]benz[d,e]isoquinolin-7-one (BBIQ), forms on
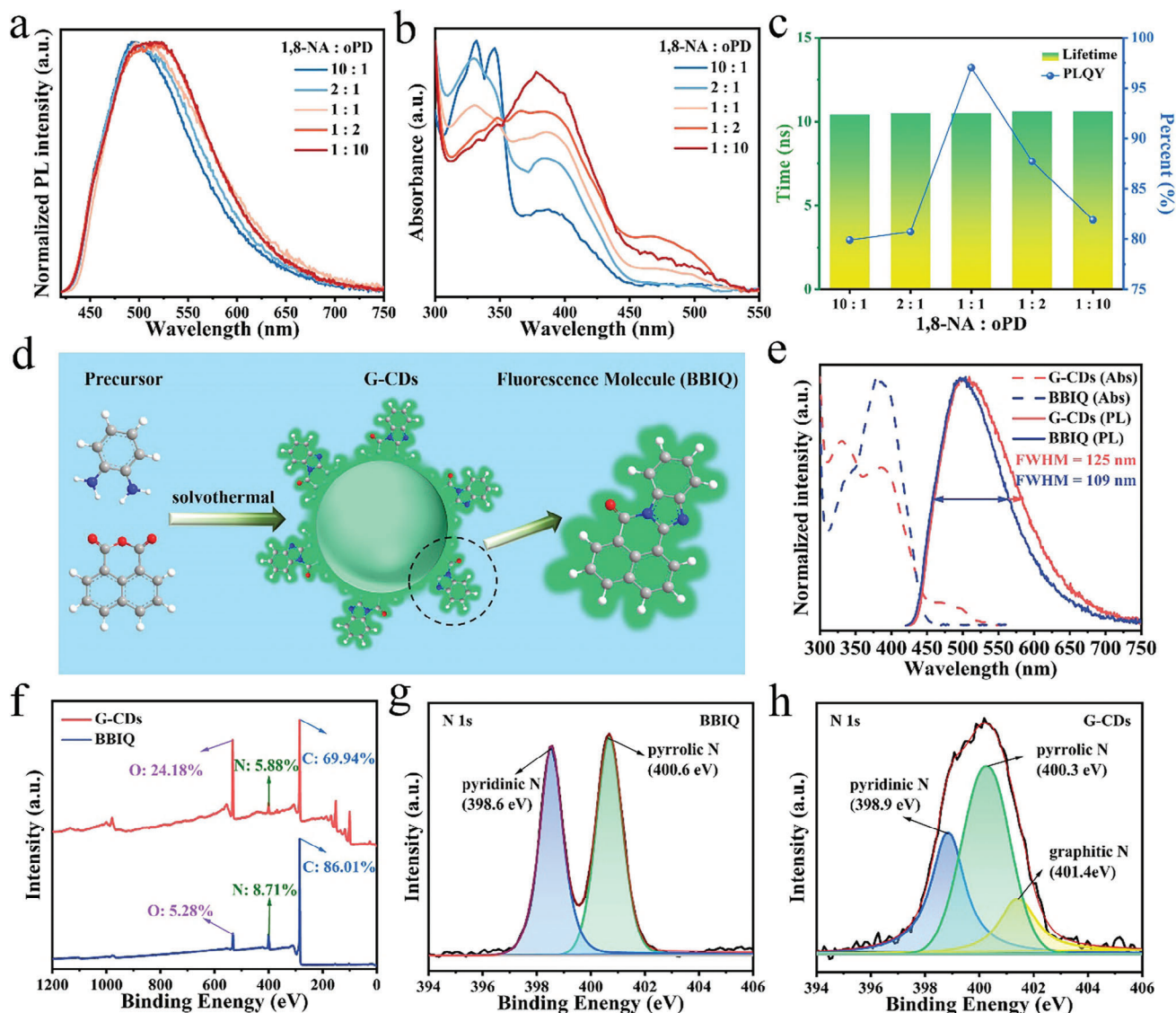
Figure 2. a) The normalized PL spectra, b) UV–vis absorption spectra, and c) PL lifetimes together with PLQY values of the CDs solutions synthesized with different precursor molar ratios. d) A schematic of the fluorescent mechanism of the G-CDs. e) Normalized PL and absorption spectra of the G-CDs and BBIQ solutions. f) The full-scan XPS spectra of the G-CDs and BBIQ. High-resolution N1s XPS spectra of (g) BBIQ and (h) G-CDs.

the surface or embedded in the carbon core during the solvothermal process (Figure 2d). Supporting this hypothesis, both G-CDs and BBIQ exhibit identical emission peaks and broadband features (Figure 2e). The absorption spectrum of BBIQ shows a strong peak near 380 nm, aligning with the fluorescence origin. Meanwhile, G-CDs display a weak absorption peak ≈480 nm, likely associated with surface states, which may contribute to the broader emission spectrum of G-CDs compared to BBIQ.[18,26] The fluorescence lifetime of BBIQ was determined to be 10.65 ns based on single-exponential decay fitting, closely matching that of G-CDs (Figure S7, Supporting Information). The PLQY of BBIQ was measured at 87.69%, slightly lower than that of G-CDs (Figure S8, Supporting Information). Furthermore, substituting oPD with p-phenylenediamine (pPD) or m-phenylenediamine (mPD) eliminated the intense green emission and resulted in

low PLQY of corresponding products, which further confirms the molecular-state-related emission mechanism of G-CDs (Figure S9, Supporting Information). Besides, the fluorescence spectra of G-CDs demonstrate solvent dependence (Figure S10, Supporting Information), with the emission peak showing a significant redshift as the solvent polarity increases. As the concentration of G-CDs in the solvent increases, the emission spectrum intensity decreases and shifts toward longer wavelengths (Figure S11, Supporting Information).

The full-scan XPS survey spectra of G-CDs and BBIQ molecules are shown in Figure 2f, with peaks observed at 284.8, 400.2, and 532.7 eV, corresponding to the C 1s, N 1s, and O 1s regions, respectively. The atomic compositions of G-CDs were calculated as 69.94% C, 5.88% N, and 24.18% O, indicating a significantly higher O/C ratio compared to BBIQ. High-resolution
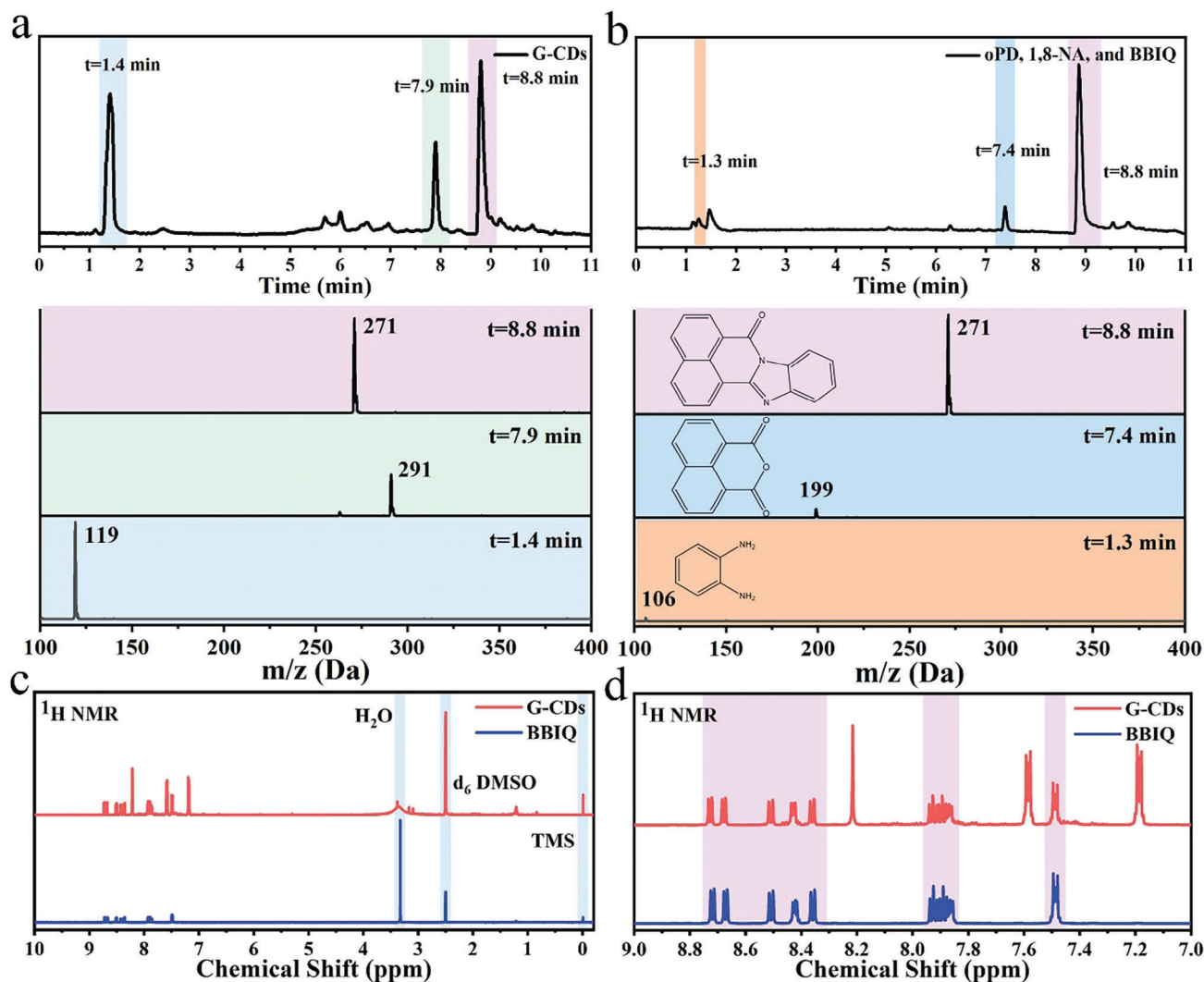
**ADVANCED
SCIENCE NEWS**

www.advancedsciencenews.com

**ADVANCED
FUNCTIONAL
MATERIALS**

www.afm-journal.de

Figure 3. a) LC-MS analysis of the synthesized G-CDs and b) the mixture of oPD, 1,8-NA, and BBIQ, showing the LC profiles (top) and the corresponding mass spectra for the peaks at various retention times (bottom). c) Comparison of the ^{1}H-NMR spectra for the synthesized G-CDs and BBIQ. d) Magnified view of the localized regions in the ^{1}H-NMR spectra for the synthesized G-CDs and BBIQ.

C 1s and O 1s spectra for both materials are shown in Figure S12 (Supporting Information). The O1s spectrum of BBIQ exhibits a single peak at 531.5 eV, corresponding to the C=O group. In contrast, the O1s spectrum of G-CDs is deconvoluted into two distinct peaks at 532.9 and 532.0 eV, attributed to C—O and C=O groups, respectively. The higher oxygen content in G-CDs aligns with additional UV–vis absorption bands observed at 330 and 480 nm, which are attributed to oxygen-containing functional groups. Further analysis of the N 1s spectra of the two samples highlights an extra peak at 401.4 eV in G-CDs, corresponding to graphitic nitrogen (Figure 2g,h). This peak complements the pyridinic nitrogen and pyrrolic nitrogen peaks observed in both samples.[27] The presence of graphitic nitrogen provides further evidence of a carbon core state in G-CDs.

To confirm that the BBIQ molecule serves as the fluorophore in G-CDs, we performed liquid chromatography-mass spectrometry (LC-MS) analysis on the purified G-CDs. The LC-MS spectra (**Figure 3a**) reveal three primary peaks in the LC trace with reten-

tion times (t) of 1.4, 7.9, and 8.8 min, corresponding to mass spectrometry (MS) peaks at m/z values of 119, 291, and 271, respectively. To identify the chemical structures of these dominant fragments, standard compounds, including 1,8-NA, oPD, and BBIQ, were analyzed under identical LC-MS conditions (Figure 3b). The LC traces for these standards show three main peaks with retention times of 1.3, 7.4, and 8.8 min, corresponding to MS peaks at m/z values of 106, 199, and 271, which are attributed to oPD, 1,8-NA, and BBIQ, respectively.

The LC-MS results for G-CDs and BBIQ demonstrate identical retention times (t = 8.8 min) and m/z values (m/z = 271), confirming that the species with m/z = 271 can be assigned to BBIQ. To further verify the presence of BBIQ in G-CDs, proton nuclear magnetic resonance (^{1}H NMR) spectroscopy was employed. The ^{1}H NMR spectra of BBIQ and G-CDs (Figure 3c,d) show matching hydrogen signals. Additionally, the G-CDs spectra display extra chemical shifts at 8.2, 7.6, and 7.2 ppm, which are attributed to the graphitized carbon core and aromatic regions.[25,29] These

**ADVANCED
SCIENCE NEWS**

www.advancedsciencenews.com

**ADVANCED
FUNCTIONAL
MATERIALS**

www.afm-journal.de

findings suggest that BBIQ chemically bonds with the carbon core, resulting in G-CDs that exhibit a fluorescence emission predominantly governed by the BBIQ molecular state.[28] This cross-linking interaction enhances the PLQY from 87.69 to 97.03%, likely due to the suppression of molecular rotation and vibration. The stability against photobleaching of BBIQ molecules and G-CDs was further evaluated under 405 nm LED light irradiation (Figure S13, Supporting Information). After 210 min of exposure, the BBIQ molecules exhibit significant photobleaching, losing 60% of their initial PL intensity. In contrast, G-CDs retain 90% of their initial PL intensity over the same duration. This superior photostability, combined with the higher PLQY of G-CDs compared to BBIQ molecules, highlights their strong potential for optoelectronic applications.

With the high PLQY of G-CDs established, we proceeded to fabricate electroluminescent devices to evaluate their performance. A conventional device structure was employed, using pure G-CDs as the emitting layer. The device structure contains an indium tin oxide (ITO) anode, poly(3,4 ethylene dioxythiophene):poly(styrenesulfonate) (PEDOT:PSS) hole-injection layer, active emission layer based on CDs, 1,3,5-tris(n-phenylbenzimidazol-2-yl)benzene (TPBi) electron-transporting layer (ETL), LiF electron-modified layer, and Al cathode was used to prepare electroluminescent device. However, these devices failed to emit light (Figure S14, Supporting Information), likely due to severe AIQ in the solid state as well as the poor electrical transport property of G-CDs. To address the adverse effects of AIQ on device performance, we incorporated the commercially available TFB as a host material, aiming to mitigate AIQ in G-CDs. Both TFB and G-CDs demonstrated good solubility in aromatic solvents, enabling the formation of uniform thin films via solution processing. As shown in Figure S15 (Supporting Information), increasing the proportion of TFB significantly enhanced the current injection level and luminance while reducing the V_t of the devices. This improvement is attributed to the excellent hole transport properties of TFB and its suitability as a high-performance blue-emitting polymer, which compensates for the poor charge transport in G-CDs. Despite these enhancements, the lack of a red component in the device limited the CRI of the resulting G-CDs-based WLEDs to 79, underscoring the need for further optimization to achieve broader spectral coverage.

To achieve high-CRI white light emission, we developed a "dual-phase CDs emitter" strategy by combining the G-CDs synthesized in this work with CDOFs exhibiting dual blue and red emission (**Figure 4**a). This approach enables the construction of high-CRI white CD-LEDs without reliance on expensive commercial host materials. The CDOFs were synthesized following our previously established solvothermal protocol using 1,3,5-benzenetricarboxylic acid, guanidinium dihydrogen phosphate, and 3,4,9,10-perylenetetracarboxylic dianhydride as precursors.[15] The resulting CDOFs displayed blue fluorescence and red phosphorescence with a PLQY of 10.03% (Figure S16, Supporting Information). Structurally, the CDOFs consist of luminescent carbon cores linked to multiple molecular chains. The integration of CDOFs into WLEDs offers several advantages: i) The reticulated structure of the CDOFs stabilizes the triplet energy levels of the carbon quantum dot core, enhancing the spin-orbit coupling between singlet and triplet states. This enables efficient red phosphorescence, which, when com-

bined with the blue fluorescence of the CDOFs and the green fluorescence of G-CDs, achieves full RGB primary colors. ii) The perylene-perylene molecular chains in the CDOFs form a regular, parallel arrangement, creating efficient π-channels for charge transport and enhancing the overall charge transport performance of the emitting layer. iii) The reticulated framework of the CDOFs mitigates AIQ in G-CDs, further improving device performance.

The PL spectra of pure G-CDs and CDOFs thin films, prepared by spin-coating with chlorobenzene as the solvent, are shown in Figures 4b,c. Compared to their solution-phase spectra, the G-CDs film exhibits a redshift in the emission peak, shifting from 500 nm to 545 nm. This spectral redshift is commonly observed in CDs and is attributed to the increased distance between the luminescent centers when transitioning from solution to thin film, leading to additional energy transfer processes.[11] For the CDOFs film, the emission peak occurs at 403 nm (Figure 4c), which is a 27 nm redshift compared to the solution-phase PL peak. This relatively modest redshift can be explained by the surrounding framework structure, which stabilizes the carbon core and prevents direct interactions that might otherwise lead to significant shifts. Furthermore, this framework structure plays a crucial role in suppressing AIQ in G-CDs when they are incorporated into the CDOFs:G-CDs composite film. As shown in Figure 4d, when G-CDs are mixed with CDOFs, the emission peak of the green component shifts to 512 nm, representing a significant improvement compared to the PL of pure G-CDs film. This enhancement supports the feasibility of the "dual-phase CDs emitter" strategy, which combines the emission properties of both types of CDs for improved device performance.

To evaluate the suitability of the thin films for use in electroluminescent devices, we assessed the morphology of the films using atomic force microscopy (AFM) measurements (Figure 4e–g). The results reveal that all three thin films—pure G-CDs, pure CDOFs, and the dual CD emitter—are uniformly smooth, with root mean square (RMS) roughness values of 0.37, 0.89, and 0.59 nm, respectively. These low roughness values indicate that the dual CDs emitter exhibits excellent film-forming properties and oil solubility. This makes the material well-suited for directly solution-processed methods.

Based on the above results, we sought to explore the potential of the "dual CDs emitter" strategy in electroluminescent WLED. As depicted in **Figure 5**a, the ultraviolet photoelectron spectroscopy (UPS) results indicate that the work function (W_F) and the highest occupied molecular orbital (HOMO) energy level of G-CDs is 3.97 and −5.30 eV, respectively. The energy level diagram of WLEDs is illustrated in Figure 5b, where the PEDOT:PSS serves as the hole transport layer, and TPBi serves as the electron transport layer. The lowest unoccupied molecular orbital (LUMO) and HOMO energy levels of CDOFs and other functional layers are taken from the literatures.[15,30] The energy levels of G-CDs fall entirely within the energy levels of CDOFs, ensuring efficient charge injection and confinement. By adjusting the ratio of CDOFs to G-CDs, we can fine-tune the emission ratio of red, green, and blue components, thereby achieving white light emission with a high CRI (Figure 5c). The device parameters of white CDs-LEDs with various CDOFs:G-CDs ratios are shown in Figure S17 and Table S1 (Supporting Information). As shown in Figure 5d, when the CDOFs to G-CDs ratio
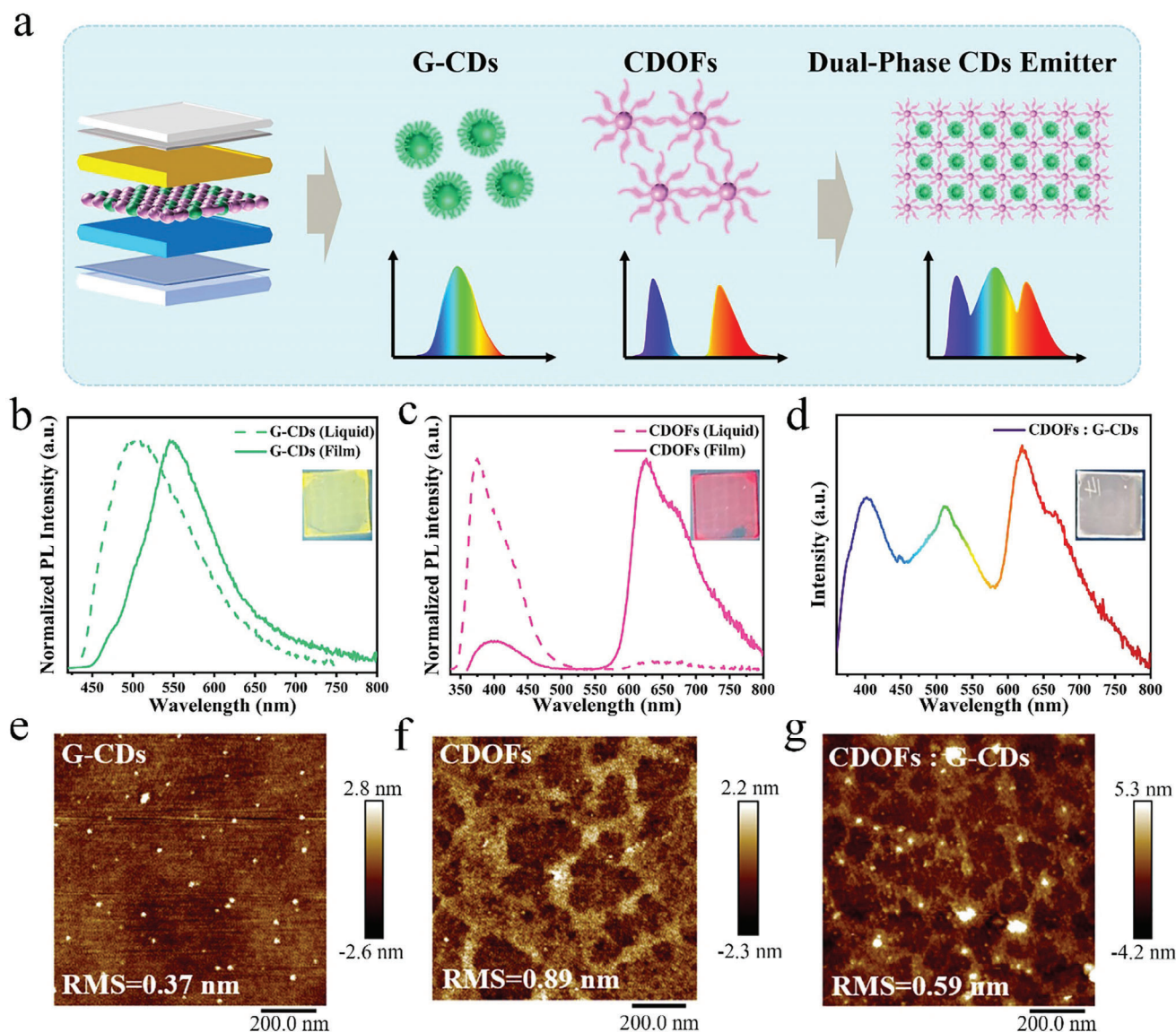
**ADVANCED
SCIENCE NEWS**

www.advancedsciencenews.com

**ADVANCED
FUNCTIONAL
MATERIALS**

www.afm-journal.de

Figure 4. a) Schematic illustration of the device architecture based on G-CDs and CDOFs as dual-phase emitters. PL spectra of b) G-CDs, c) CDOFs, and (d) CDOFs:G-CDs. Insets are the corresponding photos under UV excitation. AFM image of e) G-CDs, f) CDOFs, and g) CDOFs:G-CDs.

is 4:1, the WLED emits pure white light with Commission Internationale de l'Eclairage (CIE) coordinates of (0.32, 0.34) coupled with a high CRI of 94. This result demonstrates that high-CRI white light emission can be achieved without the need for additional commercial hosts, highlighting the potential of our "dual-phase CDs emitter" strategy for developing high-performance CDs-based WLEDs.

As shown in Figure 5e, the device achieves a maximum brightness of 644 cd m^{-2}, setting a new record for CDs-WLEDs using a pure CDs emitter. The performance parameters of these devices are compared with other reported CDs-WLEDs in Table S2 (Supporting Information). Although the values are lower than those of CDs-WLEDs based on commercial hosts, performance could be further improved by enhancing the luminescence efficiency of CDOFs and optimizing the device structure. Finally, the large-area CDs-WLEDs demonstrate bright, uniform electrolumines-

cent emission, showcasing the effectiveness of the "dual-phase CDs emitter" strategy (Figure 5f).

3. Conclusion

In summary, we synthesized G-CDs with broadband emission via a simple solvothermal treatment of 1,8-NA and oPD. Spectroscopic and structural analyses confirmed that the fluorescence mechanism of these CDs originates from the BBIQ molecular state. With their high PLQY and broad green light emission, these G-CDs hold significant potential for white light electroluminescent device applications. Building on this, we developed a novel "dual-phase CDs emitter" strategy to construct CDs-WLEDs with a high CRI. The resulting WLEDs achieved a CRI of 94, peak brightness exceeding 600 cd m^{-2}, and CIE coordinates of (0.32, 0.34). This approach delivers full-spectrum white light
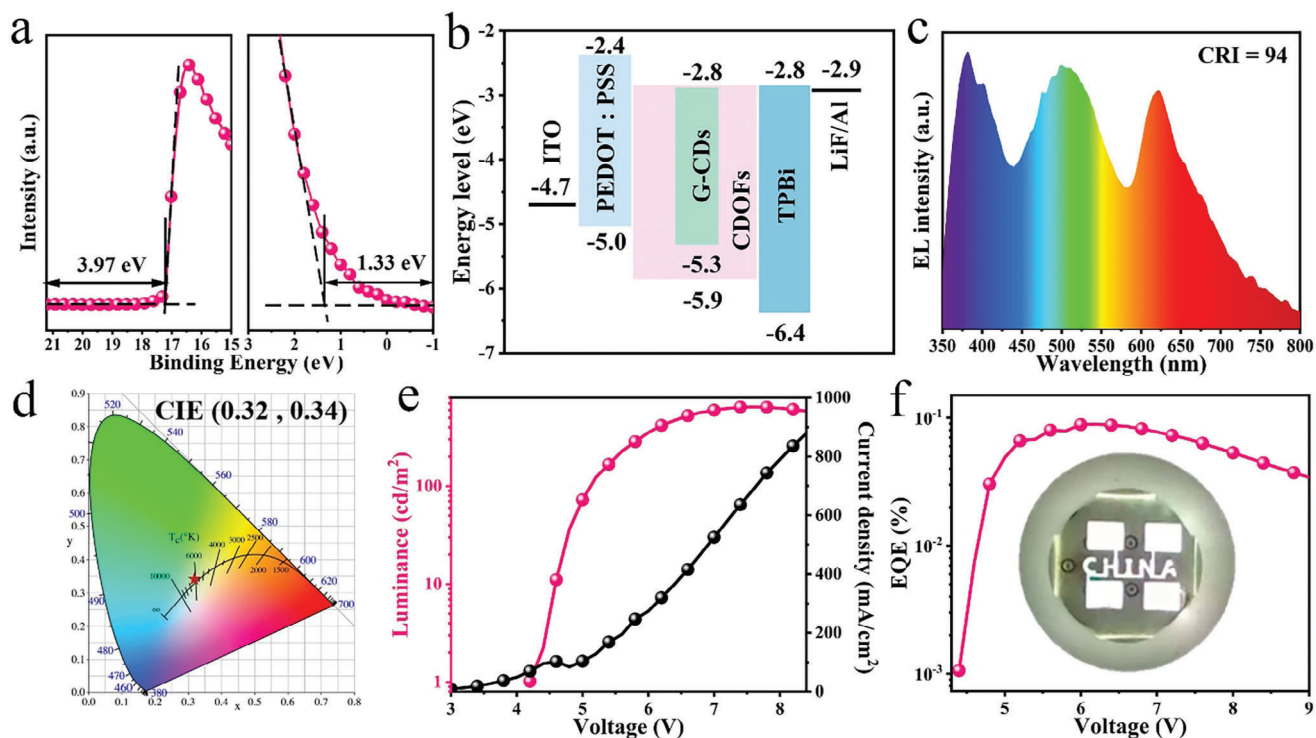
Figure 5. a) The UPS spectra of the G-CDs. b) The energy level diagram of CDs-WLEDs with dual-phase CDs emitter. c) Normalized electroluminescence spectrum and d) the Commission Internationale de l'Eclairage (CIE) coordinates for the optimized CDs-WLEDs. e) Luminance-voltage-current density (L-V-J) and f) EQE-voltage curves for the optimized CDs-WLEDs. Inset presents the photograph of CDs-WLEDs operating under a constant voltage.

emission using only two types of CDs, eliminating the need for additional commercial host materials. Our findings demonstrate a practical path toward high-performance, cost-effective, and simplified CDs-WLEDs, paving the way for further advancements in this promising field.

Supporting Information

Supporting Information is available from the Wiley Online Library or from the author.

Acknowledgements

Conflict of Interest

The authors declare no conflict of interest.

Data Availability Statement

The data that support the findings of this study are available from the corresponding author upon reasonable request.

Keywords

carbon dots, electroluminescence, full-spectrum white light, light-emitting diodes, molecular fluorescence

[1] J. Cho, J. H. Park, J. K. Kim, E. F. Schubert, *Laser Photonics Rev.* **2017**, *11*, 1600147.

[2] J. Yao, L. Xu, S. Wang, J. Song, *J. Phys. Photonics* **2022**, *4*, 042001.

[3] A. L. Efros, L. E. Brus, *ACS Nano* **2021**, *15*, 6192.

[4] Q. Lin, B. Song, H. Wang, F. Zhang, F. Chen, L. Wang, L. S. Li, F. Guo, H. Shen, *J. Mater. Chem. C* **2016**, *4*, 7223.

[5] a) Y. Gao, B. Li, X. Liu, H. Shen, Y. Song, J. Song, Z. Yan, X. Yan, Y. Chong, R. Yao, S. Wang, L. S. Li, F. Fan, Z. Du, *Nat. Nanotechnol.* **2023**, *18*, 1168; b) S. Zheng, Z. Wang, N. Jiang, H. Huang, X. Wu, D. Li, Q. Teng, J. Li, C. Li, J. Li, T. Pang, L. Zeng, R. Zhang, F. Huang, L. Lei, T. Wu, F. Yuan, D. Chen, *Sci. Adv.* **2024**, *10*, eadp8473.

[6] a) F. Yuan, S. Li, Z. Fan, X. Meng, L. Fan, S. Yang, *Nano Today* **2016**, *11*, 565; b) J. Li, X. Gong, *Small* **2022**, *18*, 2205099; c) J. Li, H. Zhao, X. Zhao, X. Gong, *Adv. Funct. Mater.* **2024**, *34*, 2404473; d) W. Dong, X. Zhang, F. Yang, Q. Zeng, W. Yin, W. Zhang, H. Wang, X. Yang, S. V. Kershaw, B. Yang, A. L. Rogach, W. Zheng, *ACS Nano* **2022**, *16*, 9679; e) F. Yang, Q. Zeng, W. Dong, C. Kang, Z. Qu, Y. Zhao, H. Wei, W. Zheng, X. Zhang, B. Yang, *Light: Sci. Appl.* **2023**, *12*, 119.

[7] H. Ding, X.-X. Zhou, Z.-H. Zhang, Y.-P. Zhao, J.-S. Wei, H.-M. Xiong, *Nano Res.* **2022**, *15*, 3548.

[8] C. Ji, Q. Han, Y. Zhou, J. Wu, W. Shi, L. Gao, R. M. Leblanc, Z. Peng, *Carbon* **2022**, *192*, 198.

[9] N. Urushihara, T. Hirai, A. Dager, Y. Nakamura, Y. Nishi, K. Inoue, R. Suzuki, M. Tanimura, K. Shinozaki, M. Tachibana, *ACS Appl. Nano Mater.* **2021**, *4*, 12472.

**ADVANCED
SCIENCE NEWS**

www.advancedsciencenews.com

**ADVANCED
FUNCTIONAL
MATERIALS**

www.afm-journal.de

[10] B. Zhao, Z. Tan, *Adv. Sci.* **2021**, *8*, 2001977.

[11] Z. Wang, N. Jiang, M. Liu, R. Zhang, F. Huang, D. Chen, *Small* **2021**, *17*, 2104551.

[12] R. Chen, Z. Wang, Q. Teng, C. Li, J. Li, L. Zeng, R. Zhang, F. Huang, L. Lei, F. Yuan, D. Chen, *Adv. Sci.* **2024**, *11*, 2404485.

[13] F. Wang, Y.-h. Chen, C.-y. Liu, D.-g. Ma, *Chem. Commun.* **2011**, *47*, 3502.

[14] B. Zhao, H. Ma, H. Jia, M. Zheng, K. Xu, R. Yu, S. Qu, Z. Tan, *Angew. Chem., Int. Ed.* **2023**, *135*, e202301651.

[15] Y. Shi, Z. Wang, T. Meng, T. Yuan, R. Ni, Y. Li, X. Li, Y. Zhang, Z. Tan, S. Lei, L. Fan, *J. Am. Chem. Soc.* **2021**, *143*, 18941.

[16] H. Ding, J.-S. Wei, N. Zhong, Q.-Y. Gao, H.-M. Xiong, *Langmuir* **2017**, *33*, 12635.

[17] N. Soni, S. Singh, S. Sharma, G. Batra, K. Kaushik, C. Rao, N. C. Verma, B. Mondal, A. Yadav, C. K. Nandi, *Chem. Sci.* **2021**, *12*, 3615.

[18] B. Lyu, H.-J. Li, F. Xue, L. Sai, B. Gui, D. Qian, X. Wang, J. Yang, *Chem. Eng. J.* **2020**, *388*, 124285.

[19] F. Yuan, Z. Wang, X. Li, Y. Li, Z. Tan, L. Fan, S. Yang, *Adv. Mater.* **2017**, *29*, 1604436.

[20] H. Ding, Y. Ji, J.-S. Wei, Q.-Y. Gao, Z.-Y. Zhou, H.-M. Xiong, *J. Mater. Chem. B* **2017**, *5*, 5272.

[21] J. Ge, Q. Jia, W. Liu, L. Guo, Q. Liu, M. Lan, H. Zhang, X. Meng, P. Wang, *Adv. Mater.* **2015**, *27*, 4169.

[22] a) S.-Y. Song, K.-K. Liu, J.-Y. Wei, Q. Lou, Y. Shang, C.-X. Shan, *Nano Lett.* **2019**, *19*, 5553; b) K.-K. Liu, S.-Y. Song, L.-Z. Sui, S.-X. Wu, P.-T. Jing, R.-Q. Wang, Q.-Y. Li, G.-R. Wu, Z.-Z. Zhang, K.-J. Yuan, C.-X. Shan, *Adv. Sci.* **2019**, *6*, 1900766.

[23] L. Ai, Y. Yang, B. Wang, J. Chang, Z. Tang, B. Yang, S. Lu, *Sci. Bull.* **2021**, *66*, 839.

[24] a) P. Li, S. Xue, L. Sun, X. Ma, W. Liu, L. An, Y. Liu, D. Qu, Z. Sun, *Small* **2024**, *20*, 2310563; b) L. Cao, M. Zan, F. Chen, X. Kou, Y. Liu, P. Wang, Q. Mei, Z. Hou, W.-F. Dong, L. Li, *Carbon* **2022**, *194*, 42.

[25] B. Wang, Z. Wei, L. Sui, J. Yu, B. Zhang, X. Wang, S. Feng, H. Song, X. Yong, Y. Tian, B. Yang, S. Lu, *Light: Sci. Appl.* **2022**, *11*, 172.

[26] H. Ding, S.-B. Yu, J.-S. Wei, H.-M. Xiong, *ACS Nano* **2016**, *10*, 484.

[27] Q. Zhang, R. Wang, B. Feng, X. Zhong, K. Ostrikov, *Nat. Commun.* **2021**, *12*, 6856.

[28] P. Li, S. Xue, L. Sun, X. Zong, L. An, D. Qu, X. Wang, Z. Sun, *Light: Sci. Appl.* **2022**, *11*, 298.

[29] B. Wang, H. Wang, Y. Hu, G. I. N. Waterhouse, S. Lu, *Nano Lett.* **2024**, *24*, 2904.

[30] Z. Wang, F. Yuan, W. Sun, H. Shi, T. Hayat, A. Alsaedi, L. Fan, Z. Tan, *Adv. Opt. Mater.* **2019**, *7*, 1901299.